
Figures and figure supplements

Loss of MGA repression mediated by an atypical polycomb complex promotes tumor progression and invasiveness

Haritha Mathsyaraja *et al*

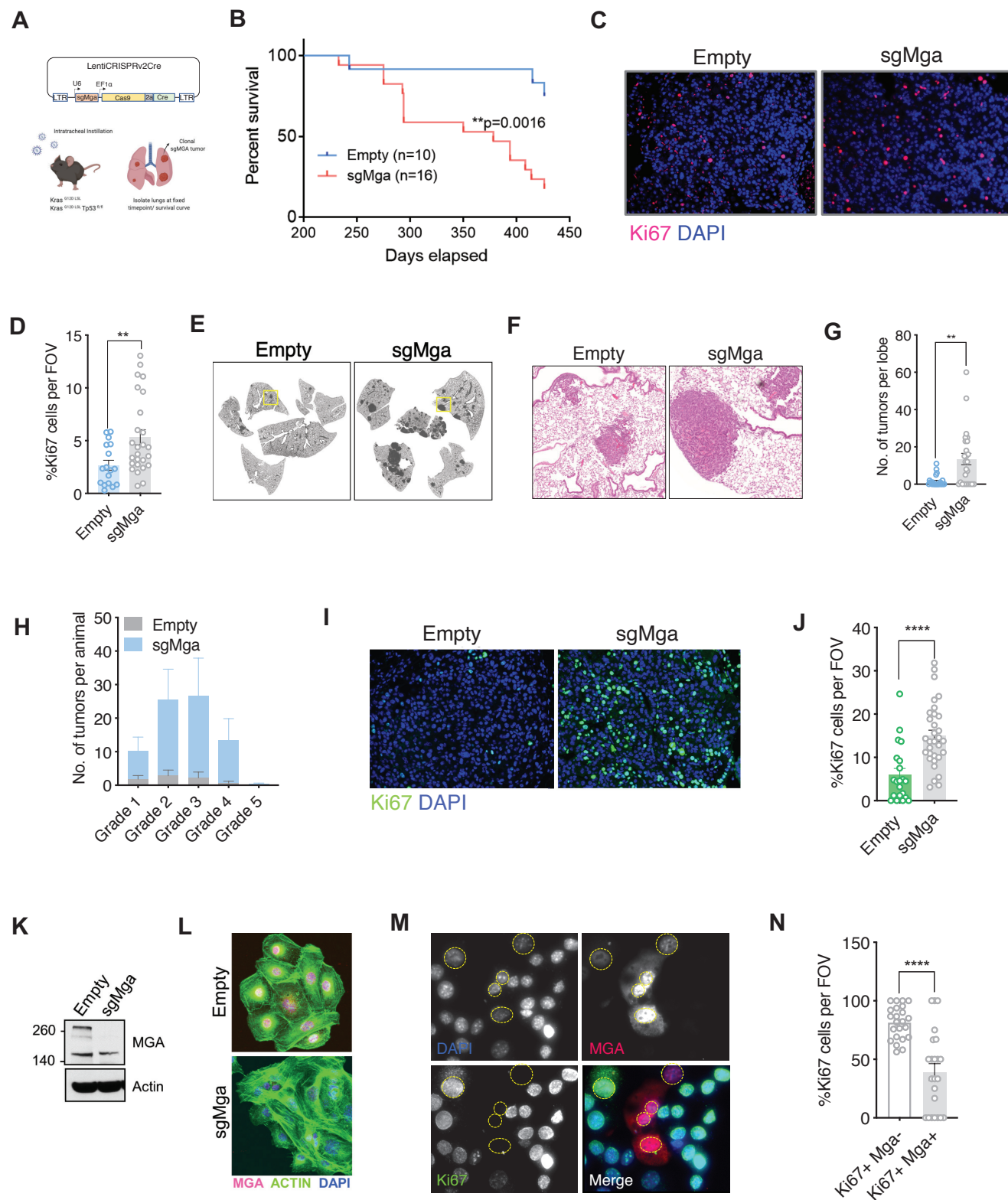


Figure 1. *Mga* inactivation in vivo leads to accelerated tumorigenesis. (A) Schematic of lentiCRISPRv2 vector and strategy used for in vivo *Kras* (K) and *Kras*, *Tp53* (KP) experiments. (B) Kaplan–Meier curve for survival in sgMga (Cre-Cas9) vs Empty (Cre-Cas9 lacking sgMga) virus-treated *Kras* mice (p-
Figure 1 continued on next page

Figure 1 continued

value computed using Log-rank test). (C) Representative micrographs and (D) quantification of Ki67 immunostaining on lung tumor tissue from Kras-sgMga and Kras empty vector infected control mice (n = 5 mice per group. **p=0.0036. Calculated using Welch's t-test assuming unequal variance). (E) Representative H and E staining of sgMga and Empty lungs from KP mice harvested 3 months post-intratracheal instillation. (F) Higher magnification of selected regions from (E) showing individual tumors in both groups. (G) Quantification of number of lesions per lobe and (H) number of lesions per grade in Empty (control) and sgMga vector treated animals (n = 5 lung lobes each from five mice per group. **p=0.001). (I) Representative images and (J) quantification of Ki67 staining to assess proliferation in KP Empty (control) and KP-sgMga lung tumors harvested 3 months post-infection (n = 32 tumors from four sgMga mice n = 21 tumors from two Empty (control) mice. ****p<0.0001. Calculated using Welch's t-test assuming unequal variance). (K) Western blot and (L) immunofluorescent staining for MGA in cell lines derived from KP tumors. (M) Representative images and (N) quantification of Ki67 and MGA co-staining in an sgMga KP line upon ectopic expression of MGA (n = 23 FOV each from three independent experiments. ****p<0.0001). All p-values calculated using a two-sided Student's t-test unless otherwise noted. Error bars represent SEM.

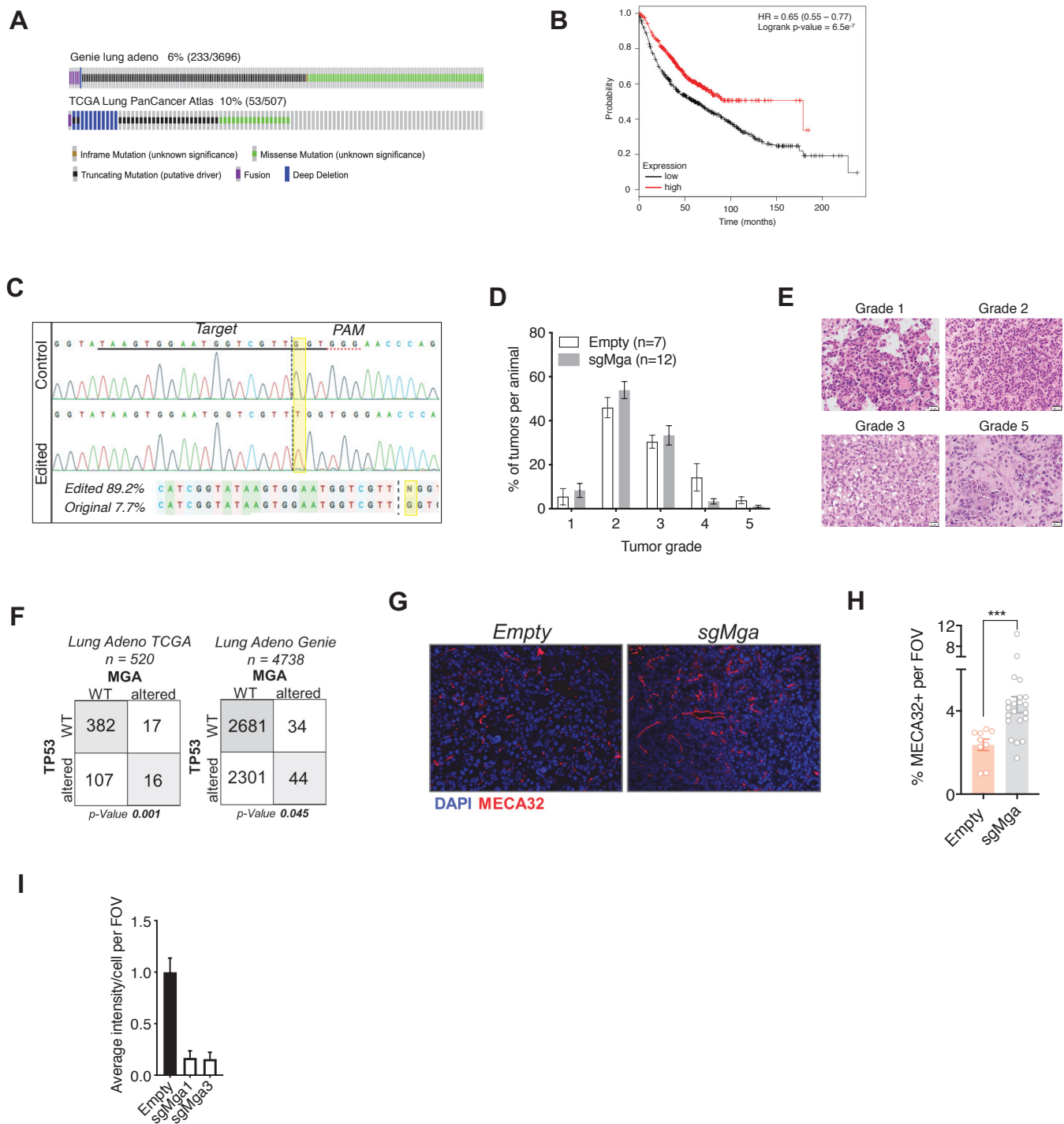


Figure 1—figure supplement 1. Mga inactivation in vivo leads to accelerated tumorigenesis. (A) Oncoprint of TCGA and GENIE consortium data on genetic alterations in MGA in lung adenocarcinoma patients. (B) Kaplan–Meier curve for survival probability based on low and high expression of MGA in lung adenocarcinoma patients (KM plotter). (C) Synthego ICE analysis of representative tumor to show percentage of indels formed as a result of sgMga CRISPR treatment. Example shows a frameshift mutation (resulting from insertion of an additional Thymidine) at a frequency of 89.2%. (D) Percentage of tumors of each grade in Empty (control) vs. sgMga-infected Kras mice harvested at endpoint. (E) Representative H and E images of tumor grades observed in Kras mice. (F) Co-occurrence of MGA and TP53 alterations in TCGA and GENIE consortia data from lung adenocarcinoma. Figure 1—figure supplement 1 continued on next page

Figure 1—figure supplement 1 continued

patients. (G) Representative micrographs and (H) quantification of pan endothelial marker MECA32 in tumors from Empty vector and sgMga vector treated KP mice harvested 3 months post-intratracheal instillation (Empty: n = 9 tumors from three mice, sgMga: n = 21 tumors from two mice. ***p=0.0003 using Welch's t-test assuming unequal variance). (I) Quantification of MGA intensity in Empty (sg-control), sgMga1 and sgMga3 KP tumor cell lines (n = 5 FOV for all groups). Error bars represent SEM.

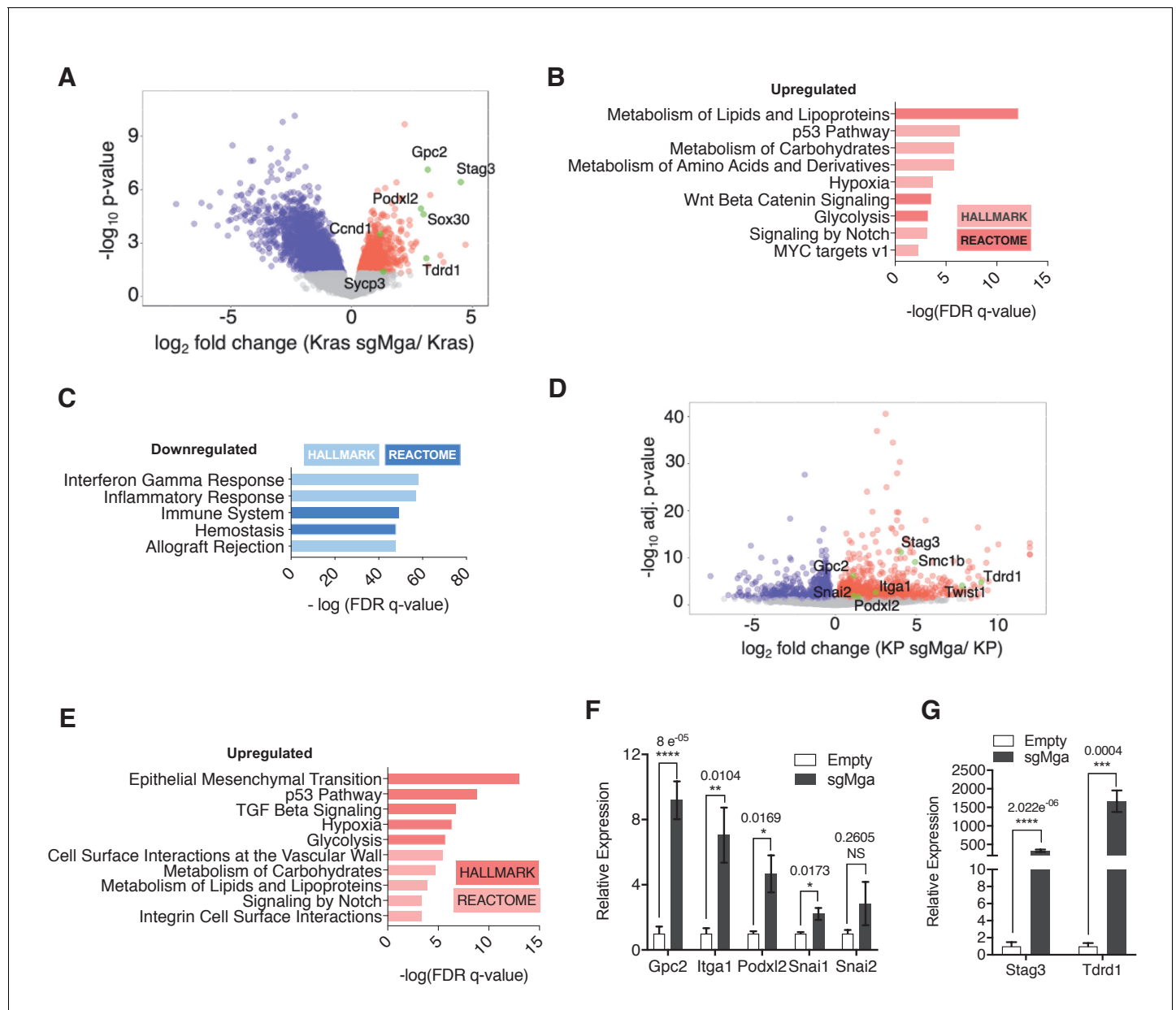


Figure 2. MGA loss leads to the de-repression of PRC1.6 and MYC targets and upregulation of pro-invasion genes. (A) Volcano plot of Kras tumor RNA profiling data comparing Kras and Kras-sgMga tumors (see **Figure 1B–D**). Upregulated pro-invasion and PRC1.6 targets highlighted in green. (B, C) Hallmark and Reactome GSEA for pathways enriched in (B) upregulated and (C) downregulated genes in Kras-sgMga tumors compared to Kras empty control tumors. (D) Volcano plot of KP cell line RNA-Seq data showing PRC1.6 and pro-invasive genes in green ($n = 2$ cell lines in triplicate for KP control and 3 cell lines in triplicate for KP-sgMGA). (E) Hallmark and Reactome analysis of genes upregulated in KP-sgMga vs. control KP empty cell lines. (F, G) qPCR on Empty and sgMga KP lines to confirm levels of (F) pro-invasive and (G) PRC1.6 meiotic targets ($n = 6$ for each – 2 sets of RNA [biological replicates] from three different lines for sgMga and Empty). p-values for individual genes indicated in figure. All p-values calculated using a two-sided Student's t-test. Error bars represent SEM.

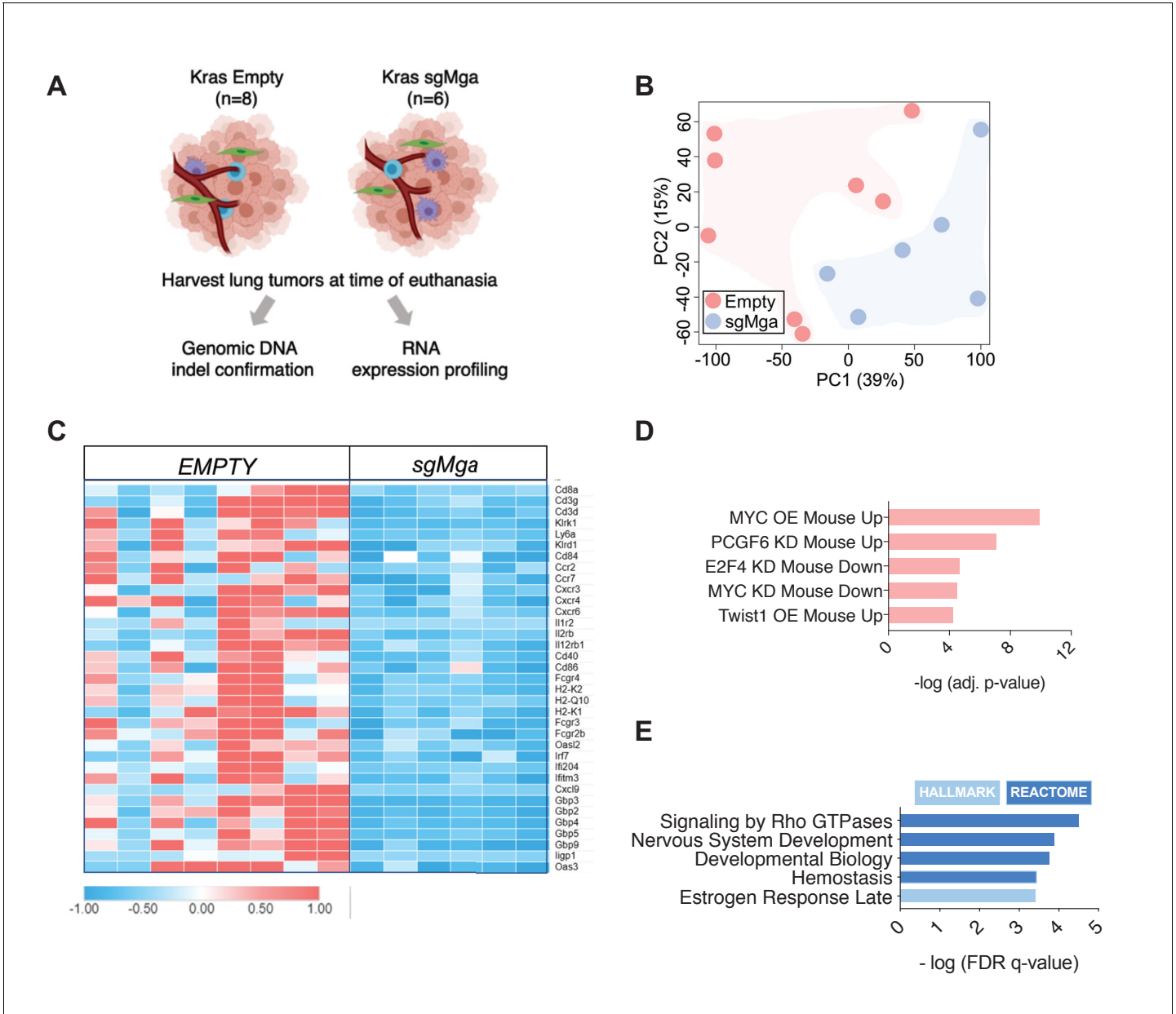


Figure 2—figure supplement 1. MGA loss leads to the de-repression of PRC1.6 and MYC targets and upregulation of pro-invasion genes. (A) Schematic depicting workflow of Kras tumor RNA-Seq. (B) PCA of Kras-sgMGA and Empty tumor RNA-Seq (n = 8 Empty, n = 6 sgMga). (C) Heatmap of downregulated immune cell and inflammation related transcripts in Kras-sgMga tumors compared to Empty. (D) Transcription Factor Perturbation datasets enriched in sgMGA KP upregulated genes (using Enrichr). (E) GSEA of genes downregulated upon loss of MGA in KP lines.

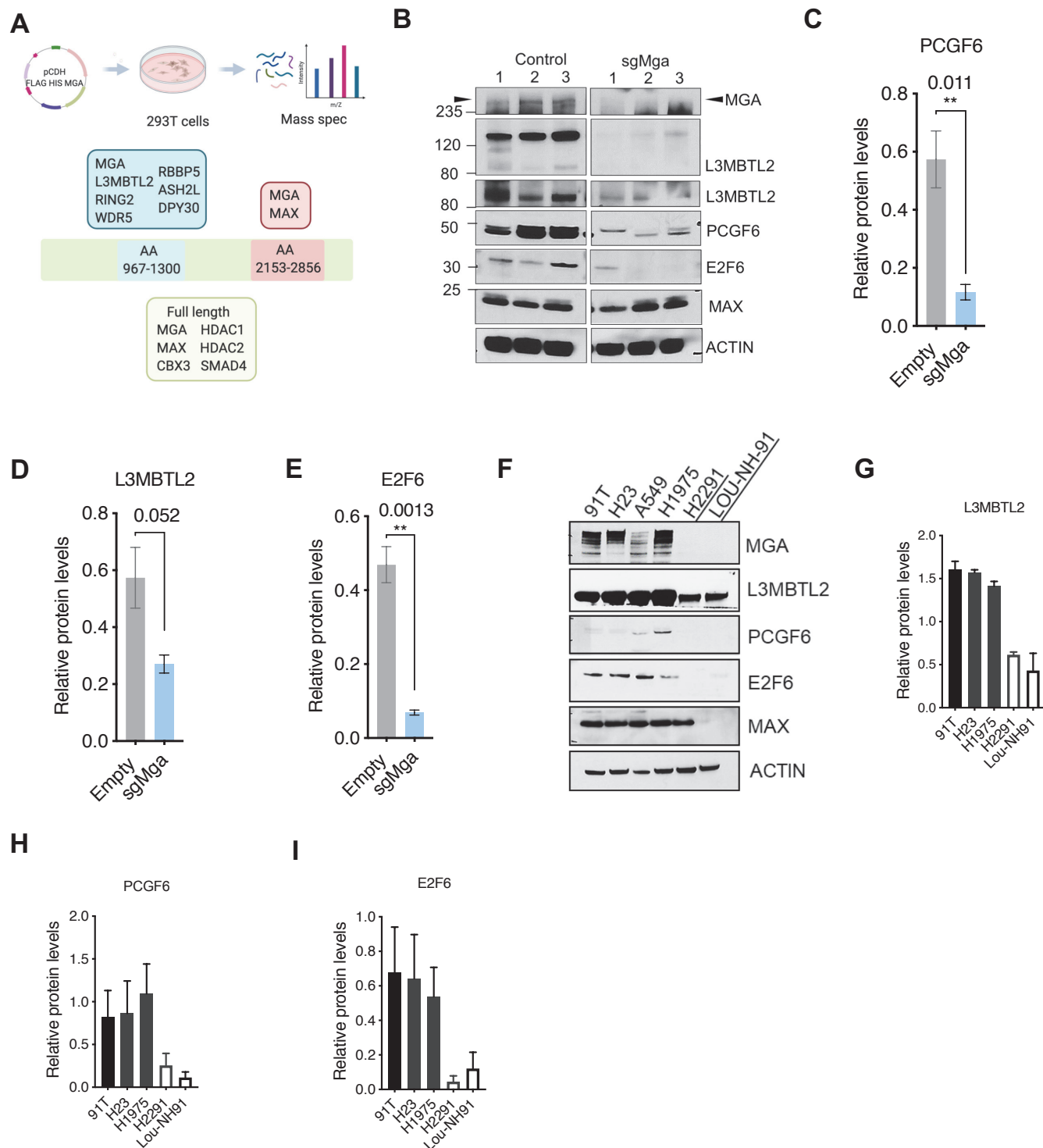


Figure 3. MGA binds and stabilizes PRC1.6 complex members in lung cancer cells. **(A)** Mass spectrometric analysis of proteins interacting with FLAG-His-double tagged full-length MGA or isolated aa967–1300 (encompassing the DUF4801 region) and aa2153–2853 (encompassing the bHLHZ domain) segments of MGA. Confirmed interactors shown shaded in color (protein prophet score > 0.9). **(B)** Representative immunoblot to show protein levels of MGA, L3MBTL2 (lower panel to show L3MBTL2 at higher exposure), PCGF6, E2F6, and MAX in control and sgMga mouse KP lines (n = 3 individual cell lines for control and sgMga). **(C–E)** Densitometry of indicated PRC1.6 members, in control and sgMGA KP lines. **(F)** Representative immunoblots for the

Figure 3 continued

indicated proteins in MGA WT and mutant human lung adenocarcinoma cell lines. (G–I) Quantification of protein levels of the indicated proteins in MGA WT (black bars) vs. MGA mutant (white bars) lung cancer lines. For densitometry, three independent western runs were used for each comparison. Error bars represent SEM.

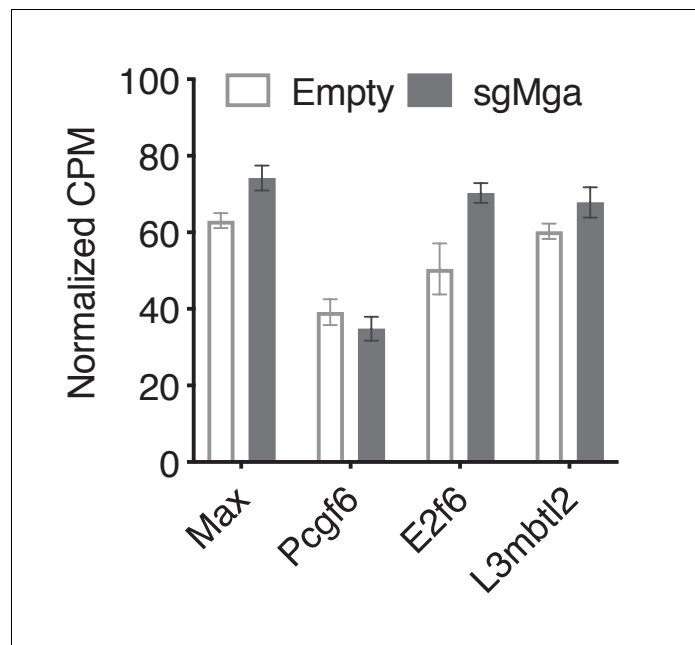


Figure 3—figure supplement 1. PRC1.6 complex member mRNA levels unchanged upon MGA loss in lung cancer cells. Normalized CPM values for PRC1.6 member RNAs in KP cells (n = 2 empty lines in triplicate, n = 3 sgMga lines in triplicate). Error bars represent SEM.

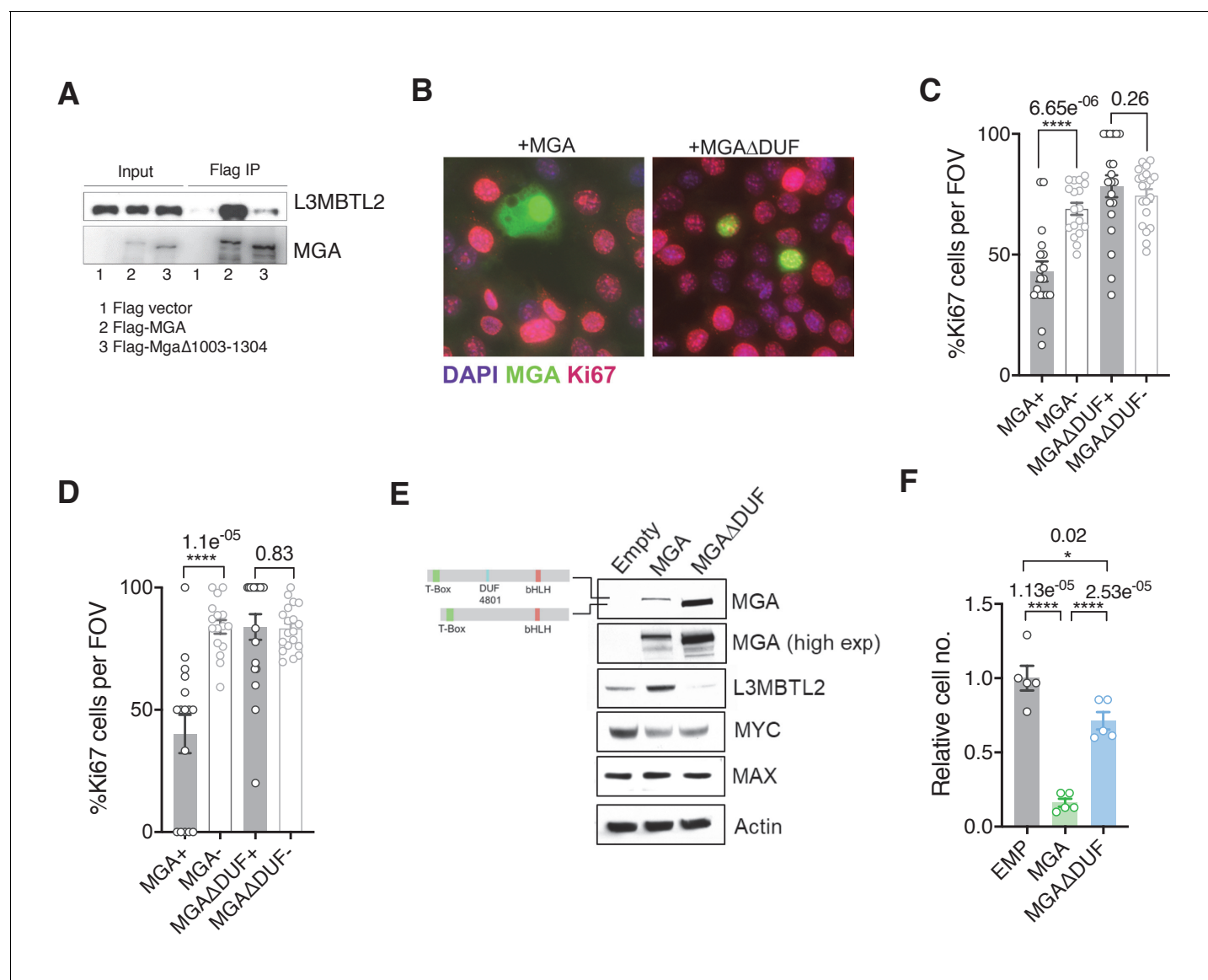


Figure 4. The region containing the DUF4801 domain is critical for MGA's tumor suppressive function. (A) Immunoblot showing co-immunoprecipitation of L3MBTL2 with full length or MGAΔ1003–1304 (ΔDUF). (B) Representative co-staining for Ki67 and MGA deficient mouse KP cells expressing MGA or MGAΔ1003–1304 (ΔDUF). (C, D) Quantification of Ki67+ cells in two independent KP-sgMga lines: (C) H8712 T3 (n = 18 FOV MGA, n = 20 FOV MGAΔDUF from four biological replicates each) and (D) H8638 (n = 17 FOV MGA, n = 20 FOV MGAΔDUF from at least four biological replicates each). (E) Immunoblots of ectopic expression of MGA or MGAΔDUF in LOU-NH-91 human lung squamous carcinoma cell line. (F) Relative growth of MGA and MGAΔDUF expressing LOU-NH-91 cells (n = 5 replicates across three independent experiments for each group). All p-values calculated using a two-sided Student's t-test unless otherwise noted (*p<0.05, ****p<0.0001). Error bars represent SEM.

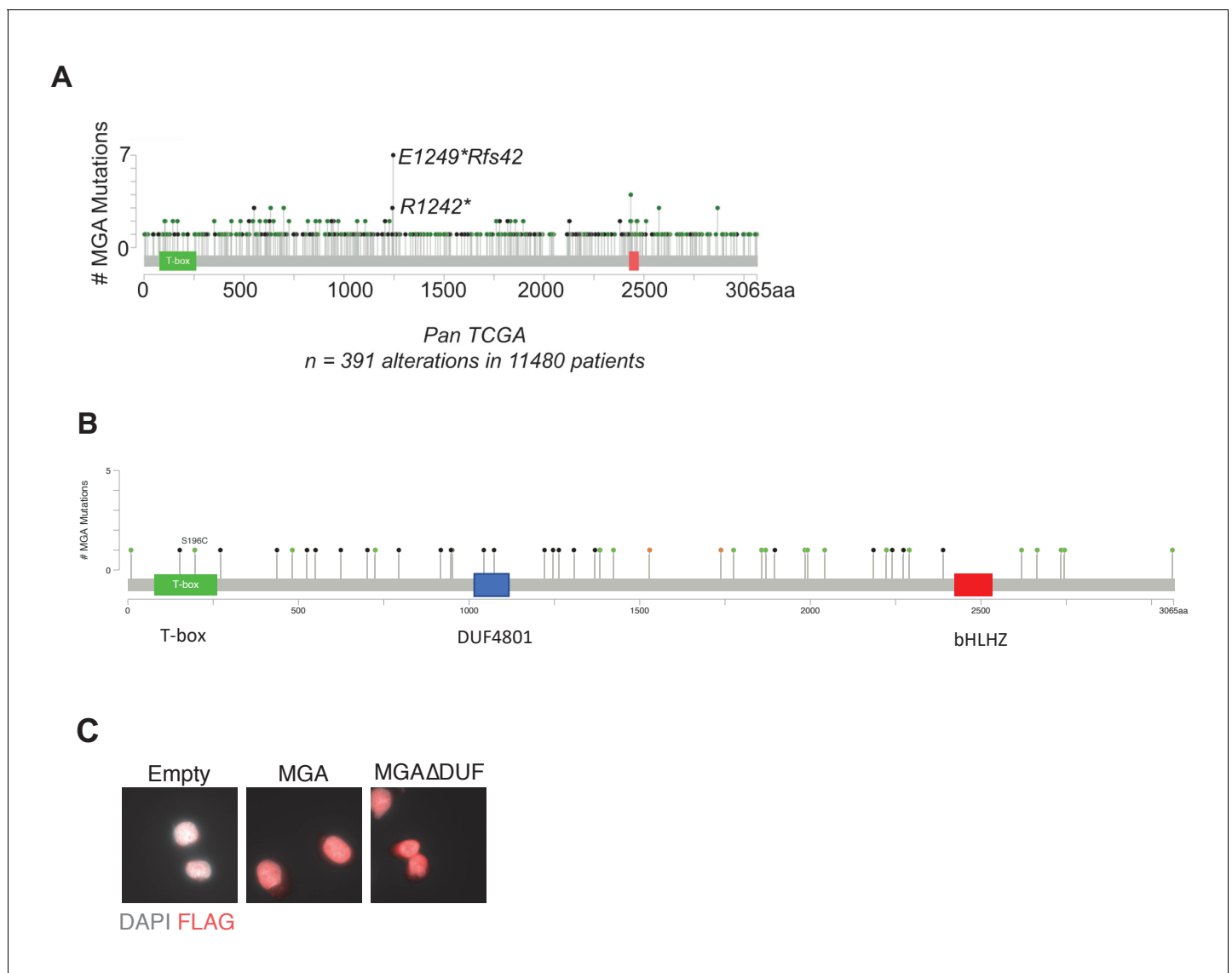


Figure 4—figure supplement 1. Cancer associated mutations within MGA. (A) Frequently occurring mutations in MGA across pan-cancer TCGA. (B) Mutations occurring within MGA in TCGA LUAD patients: black and green lollipop represent truncating mutations (black: nonsense codons; tan: splice site mutations leading to reading frame shifts), green indicates missense mutations of unknown functional consequences; (C) immunostaining for FLAG in FLAG-MGA and FLAG-MGA Δ DUF mutant expressing cells.

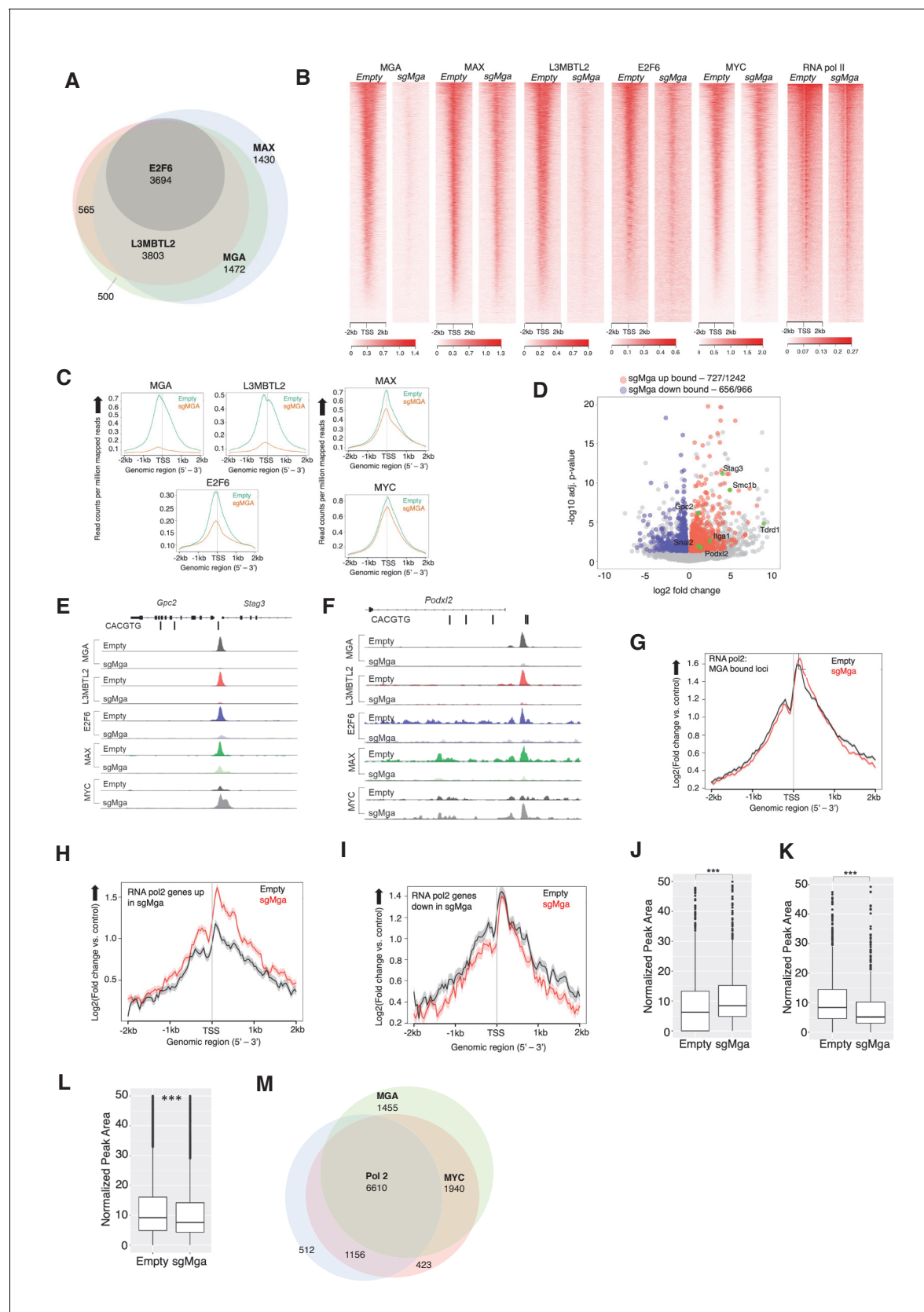


Figure 5. MGA is essential for PRC1.6 genomic binding in tumor cells. (A) Venn diagram showing overlap between MAX, MGA, E2F6, and L3MBTL2 bound genes in KP cells. (B) Heatmaps showing genome-wide promoter proximal (±2 kb) binding by the indicated transcription factors in control and Figure 5 continued on next page

Figure 5 continued

sgMga KP cells. **(C)** Meta-plots of occupancy by the indicated transcription factors in Empty and sgMga KP cells. **(D)** Volcano plot of differentially expressed genes that are directly bound by MGA (red and blue dots indicate bound genes, up and down as indicated; green dots with labels indicate genes functionally implicated in MGA activity). **(E, F)** representative tracks for MGA, L3MBTL2, E2F6, MAX, and MYC binding at the **(E)** Stag3/Gpc2 promoter and **(F)** Podxl2 loci in KP cells and sgMGA KP cells. **(G–I)** Meta-plots of RNA pol2 enrichment at the TSS ± 2 kb in sgMGA KP cells (red lines) vs KP cells with wild-type MGA (black lines) at **(G)** MGA-bound genes, **(H)** genes upregulated, and **(I)** genes downregulated in sgMGA KP cells. **(J–L)** Box plots of RNA pol2 peak areas at TSS ± 2 kb in KP vs sgMGA KP cells for **(J)** loci upregulated (p -value=2.1e-07), **(K)** loci downregulated (p =1.6e-06). The p -values in **(J–L)** calculated by Welch two sample t-test. **(L)** Box plots of RNA pol2 peak areas at MYC-bound loci in KP and sgMGA-KP cells (p =8.7e-05). **(M)** Venn diagram depicting the numbers of genes bound by RNA polymerase II, MYC, and MGA and their extent of overlap in KP cells.

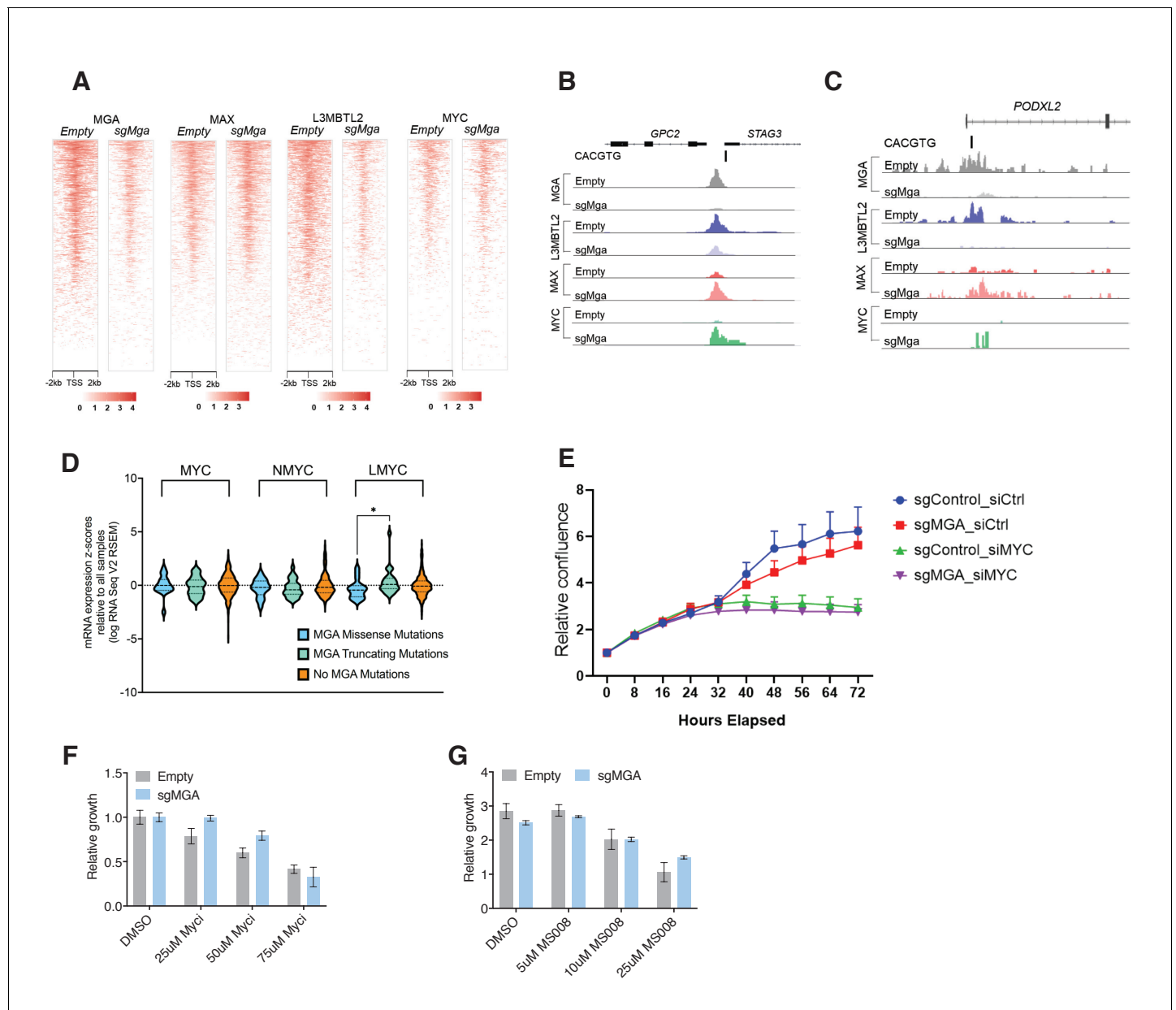


Figure 5—figure supplement 1. MGA, PRC1.6, and MYC binding and activity in human and murine LUAD-derived cells. (A) Cut and Run generated heatmaps showing genome-wide promoter proximal (± 2 kb) binding by the indicated transcription factors in control (empty) and sgMga A549 human LUAD cells. (B, C) Tracks from the indicated genes upregulated by MGA loss: (B) Peaks for MGA, L3MBTL2, MAX, and MYC occupancy at the Stag3/Gpc2 promoter in A549 cells; (C) MGA, L3MBTL2, MAX, and MYC occupancy at the *PODXL2* promoter in A549 cells. (D) TCGA data for patient LUADs profiling expression levels for MYC, MYCN, and MYCL in samples containing missense, truncation, or no mutations within MGA (see Materials and methods for details of analysis). (E) Incucyte cell counts over a 72 hr time period following plating of the indicated KP cell lines. Cells were treated with siRNA against MYC (siMYC) or control siRNAs (siCtrl). MGA loss and MYC downregulation were verified by immunoblot. (F) Growth of Control (empty) and sgMGA A549 human LUAD cell line treated with indicated concentrations of the Myc-Max dimerization inhibitor 10058-F4. Growth shown is relative to the DMSO treated control cells (set to 1.0). (G) Growth of A549 tumor cell lines: control (empty) A549 cells and sgMGA-A549 cells treated with MS2-008, a probe that forces MAX homodimerization and blocks MYC-MAX mediated transcription.

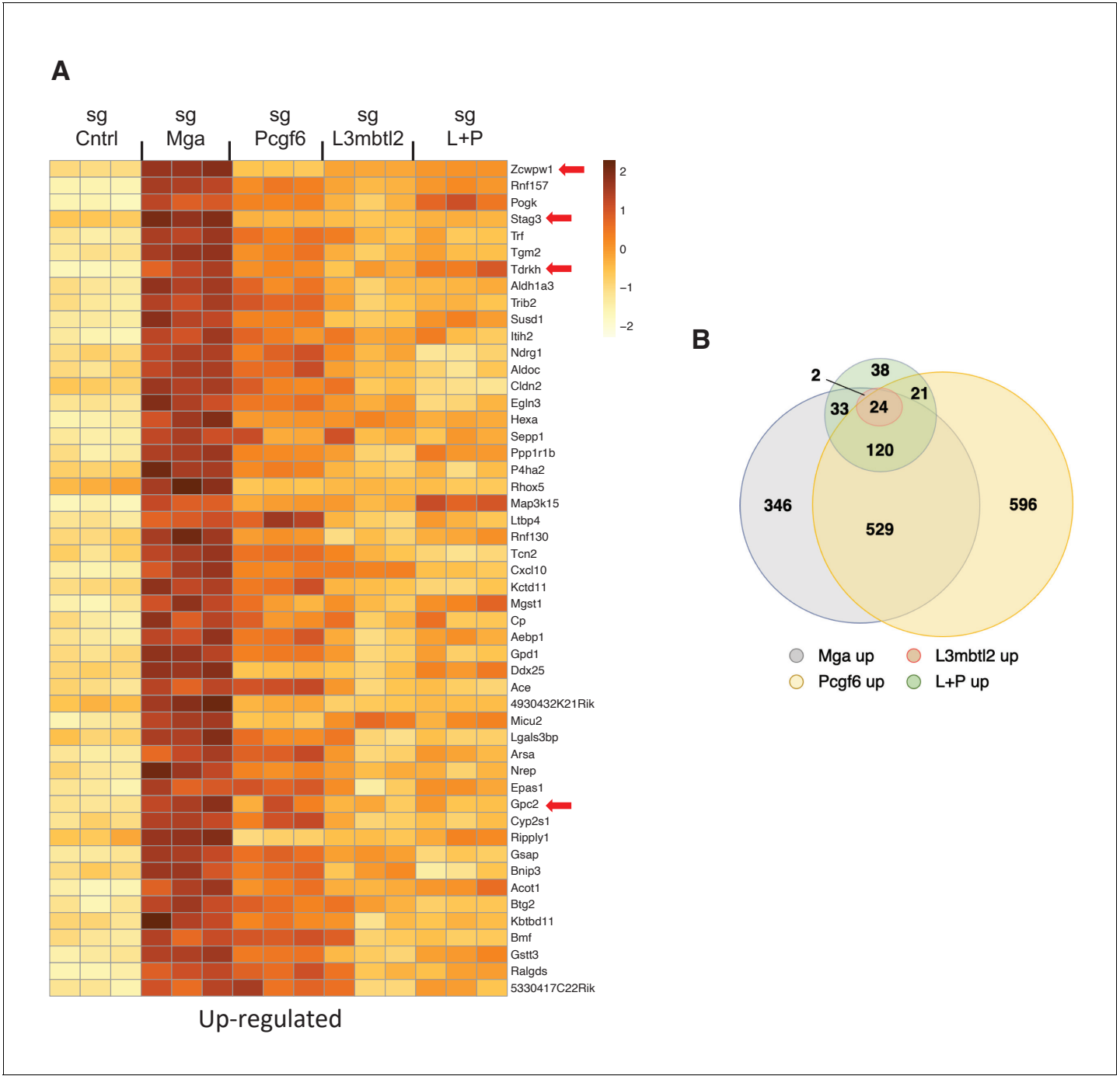


Figure 6. PRC1.6 complex subunits contribute to MGA mediated repression. **(A)** Heat map of 50 top upregulated RNAs in KP tumor cell line treated with sgControl, sgMga, sgL3MBTL2, and sgPCGF6 +sgL3MBTL2 as determined by RNA-Seq. Differential expression of RNAs ranked according the adjusted p-value in the sgMga sample, n = 3 for each sgRNA. **(B)** Venn diagram indicate extent of overlap among upregulated genes from the different CRSPR deletions shown in **(A)**. Genes with adjusted p-value<0.05 were included.

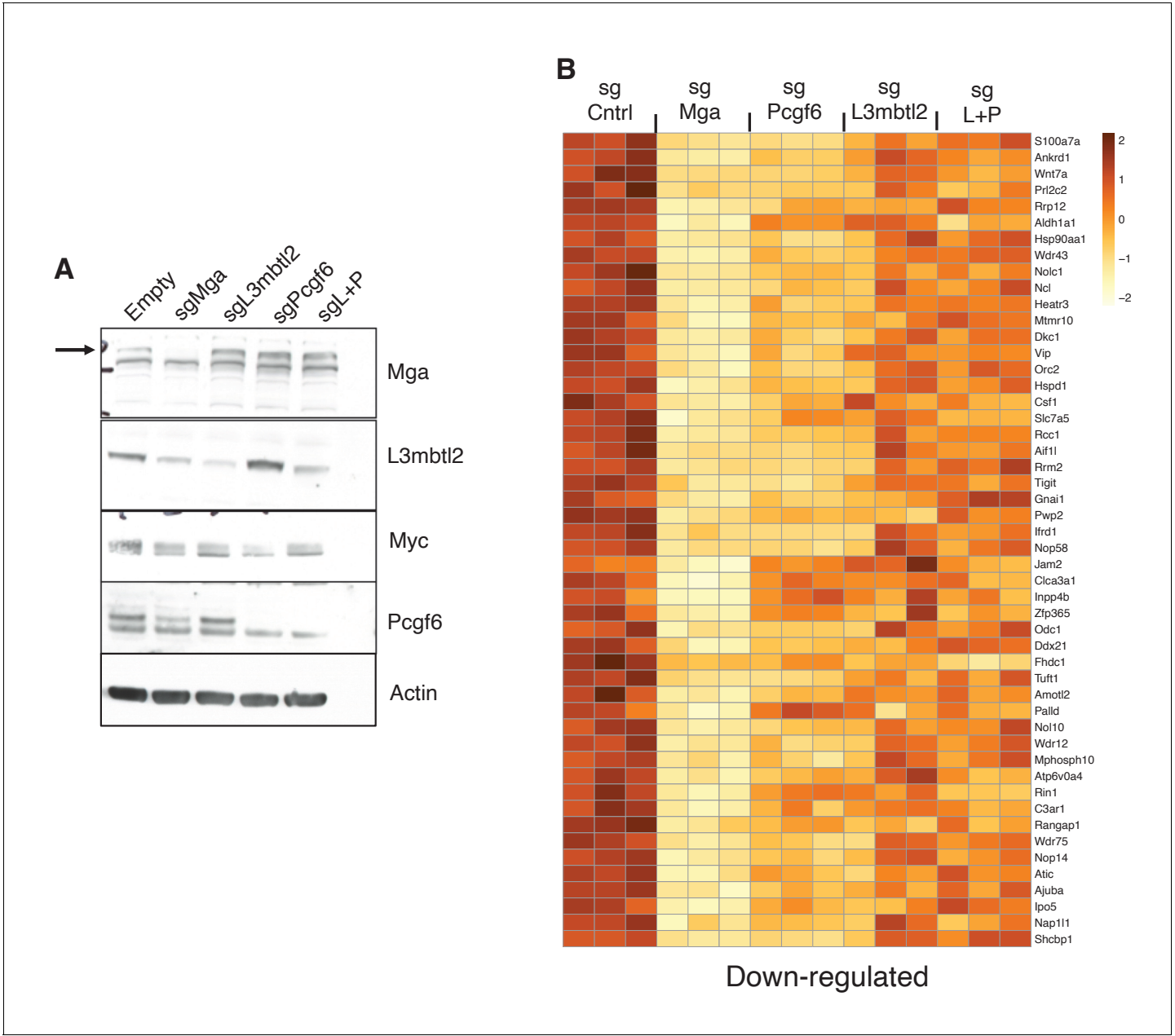


Figure 6—figure supplement 1. PRC1.6 complex subunits contribute to MGA mediated activation. **(A)** Immunoblot of the indicated proteins following treatment with the indicated sgRNA. sgL+P = sgL3MBTL2 and sgPCGF6 **(B)** Heat map of 50 top downregulated RNAs in KP tumor cell line treated with sgControl, sgMga, sgL3MBTL2, and sgPCGF6+sgL3MBTL2 (sgL+P) as determined by RNA-Seq. Differential expression of genes ranked according the adjusted p-value in the sgMga sample, n = 3 for each sgRNA.

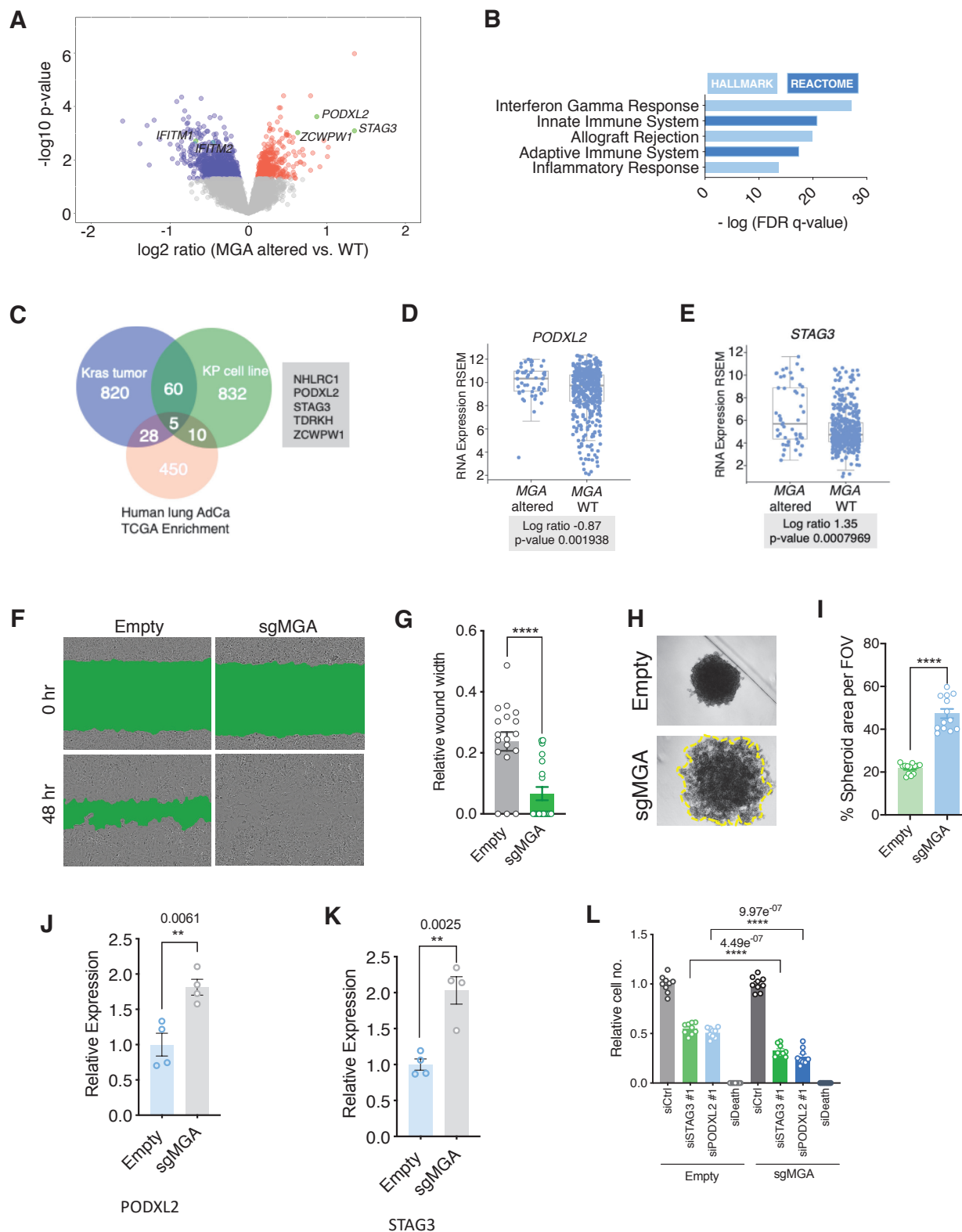


Figure 7. MGA loss correlates with activation of *STAG3* and *PODXL2* in human lung cancer and results in a pro-invasive phenotype in vitro. (A) Volcano plot of transcripts that are differentially expressed in MGA altered (n = 52) vs. WT (n = 455) from pancancer TCGA lung adenocarcinoma data. Figure 7 continued on next page

Figure 7 continued

Representative genes highlighted in green. (B) Hallmark and Reactome analysis of genes downregulated in MGA altered patients vs. non-altered (p-value cutoff < 0.05). (C) Venn diagram depicting overlap between genes upregulated in the mouse Kras tumor, KP cell line, and Human lung TCGA data with MGA alterations. (D, E) Log ratios of (D) PODXL2 and (E) STAG3 expression in MGA altered vs. WT lung adenocarcinoma patients (TCGA, 2014). (F) Representative wound widths and (G) quantification of wound width at 48 hr in Empty and sgMGA wells (n = 18 Empty, n = 20 sgMGA. ****p=4.77e⁻⁰⁵). (H) Spheroid formation and (I) quantification in Empty and sgMGA A549 lines (quantification at Day 6, n = 13 spheroids for each from three independent experiments. ****p=4.89e⁻¹¹). (J, K) qPCR for (J) PODXL2 and (K) STAG3 expression in Empty and sgMGA A549 cells (n = 4 replicates for each condition). (L) Cell growth upon siRNA knockdown of STAG3 and PODXL2 in A549 Empty and sgMGA cells (n = 3 replicates from three independent experiments for each group). All p-values calculated using a two-sided Student's t-test unless otherwise noted. Error bars represent SEM.

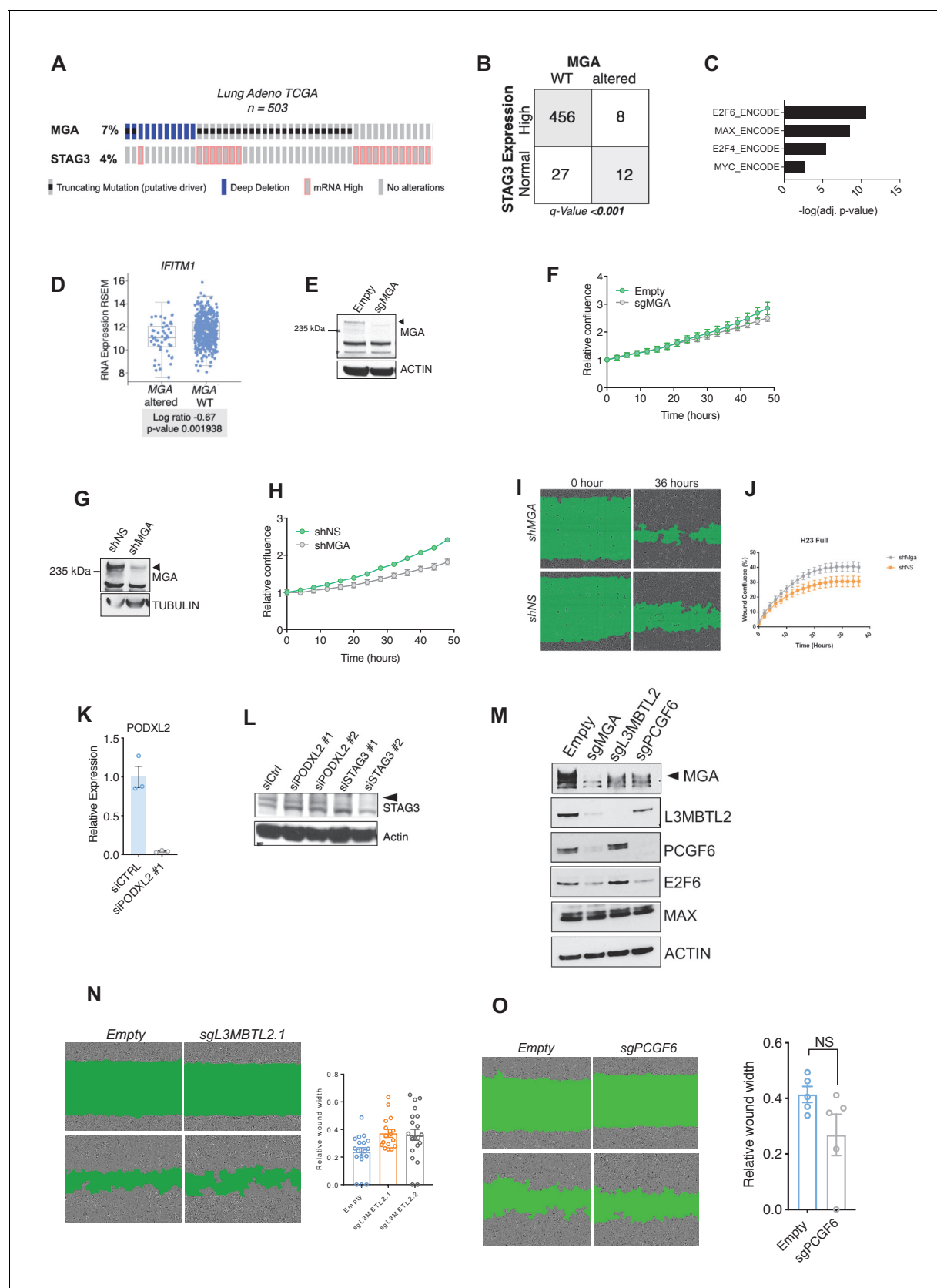


Figure 7—figure supplement 1. Manipulation of MGA in human lung cancer cell lines results in a pro-invasive phenotype and activation of PRC1.6 targets. (A) Genetic alteration in MGA and expression changes in STAG3 in human lung adenocarcinoma. (B) Co-occurrence of STAG3 ‘mRNA high’ Figure 7—figure supplement 1 continued on next page

Figure 7—figure supplement 1 continued

expression' and MGA alterations in TCGA lung adenocarcinoma data. (C) ChEA of genes overexpressed in MGA altered cases vs. WT. (D) Expression of IFN signaling gene IFITM1 in MGA altered vs. WT lung adenocarcinoma patients. (E) Immunoblot of MGA levels in sgMGA and Empty vector transduced A549 human lung adenocarcinoma cells. (F) Growth curve of Empty and sgMGA A549 cells cultured in complete media. (G) Immunoblot of MGA levels in control non-silencing shRNA (shNS) and shMGA NCI-H23 lung adenocarcinoma cells. (H) Growth curve of shMGA and non-silencing control NCI-H23 cells. (I) Wound width at 36 hr and (J) kinetics of wound closure in shNS and shMGA transduced NCI-H23 cells. (K) qPCR for PODXL2 in siCTRL vs. siPODXL2#1 transfected A549 Empty cells (n = 3 for each condition). (L) Immunoblot for STAG3 levels in siCTRL, siPODXL2, and siSTAG3 transfected A549 empty cells. All p-values calculated using a two-sided Student's t-test unless otherwise noted. Error bars represent SEM. (M) Immunoblot for MGA, L3MBTL2, E2F6 and PCGF6 in sgMGA, sgL3MBTL2, sgPCGF6, and control A549 cells. (N) Scratch wound assay comparing sgL3MBTL2 and Empty A549 cells. (O) Scratch wound assays comparing sgPCGF6 and Empty A549 cells. Error bars represent SEM.

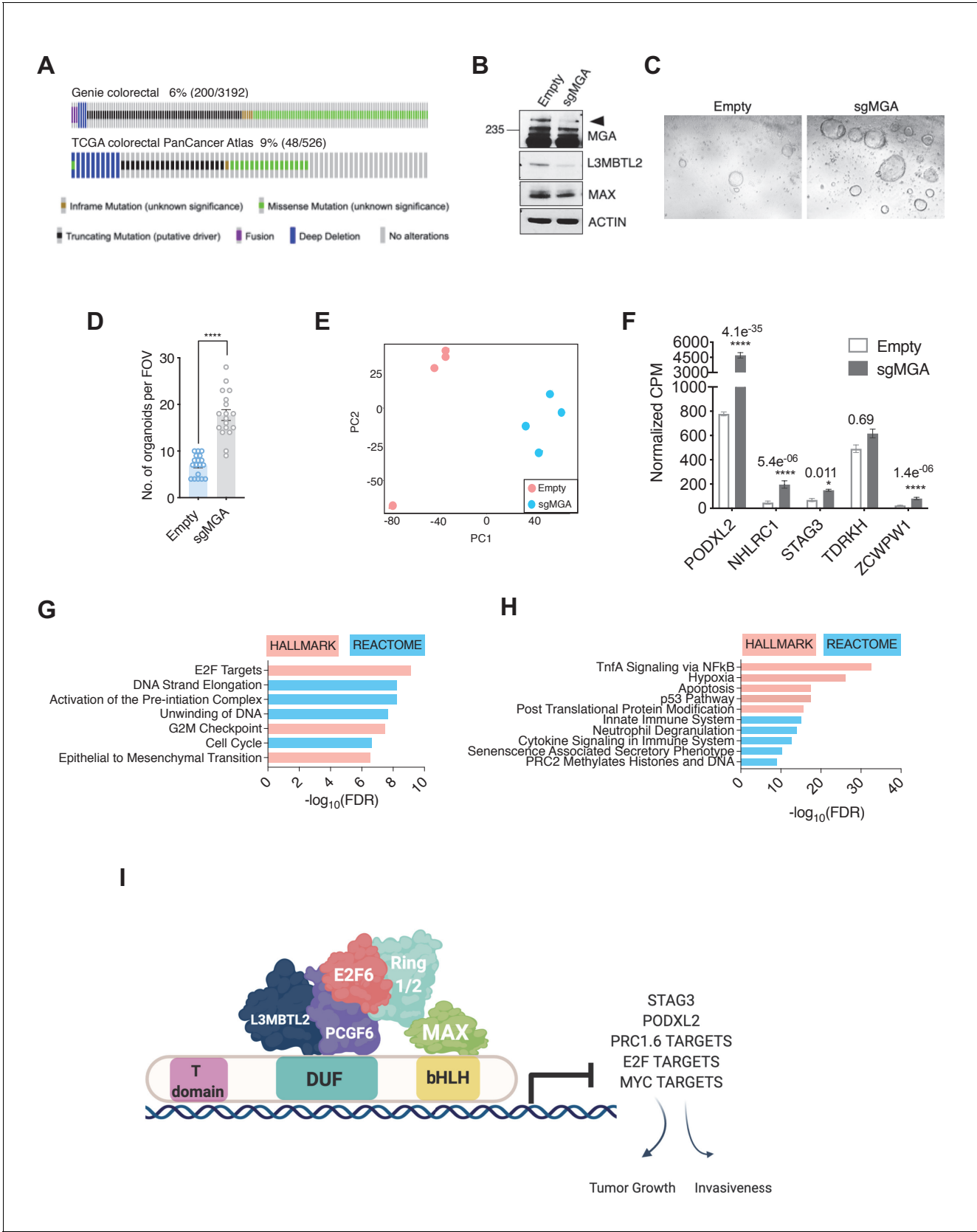


Figure 8. MGA has tumor suppressive functions in colorectal cancer. (A) GENIE and TCGA consortium data depicting alterations at the MGA locus in colorectal cancer. (B) Western blot for MGA, L3MBTL2, and MAX in Empty and sgMGA normal colon organoids. (C) Representative images and (D) Figure 8 continued on next page

Figure 8 continued

quantification of normal human colon organoid growth from single cells following MGA inactivation using CRISPR (* $p=8.84e^{-10}$. Two-sided Student's t-test, $n = 18$ FOV across six biological replicates). (E) PCA plots for Empty and sgMGA organoids ($n = 4$ biological replicates for each). (F) Normalized CPM values for MGA target genes in Empty and sgMGA organoids ($n = 4$ biological replicates for each). GSEA Hallmark and Reactome analysis for genes (G) upregulated and (H) downregulated upon MGA loss in colon organoids ($FDR < 0.05$, $LFC > 1.5$). (I) Proposed mechanism of MGA mediated tumor suppressive effects: MGA acts as a scaffold and stabilizes atypical PRC1.6 members, including L3MBTL2. Under normal conditions, this results in the repression or transcriptional attenuation of thousands of genes. During malignant progression, perturbation of MGA expression leads to the upregulation of growth-promoting and pro-invasive PRC1.6, MYC, and E2F targets in a tissue-specific manner.

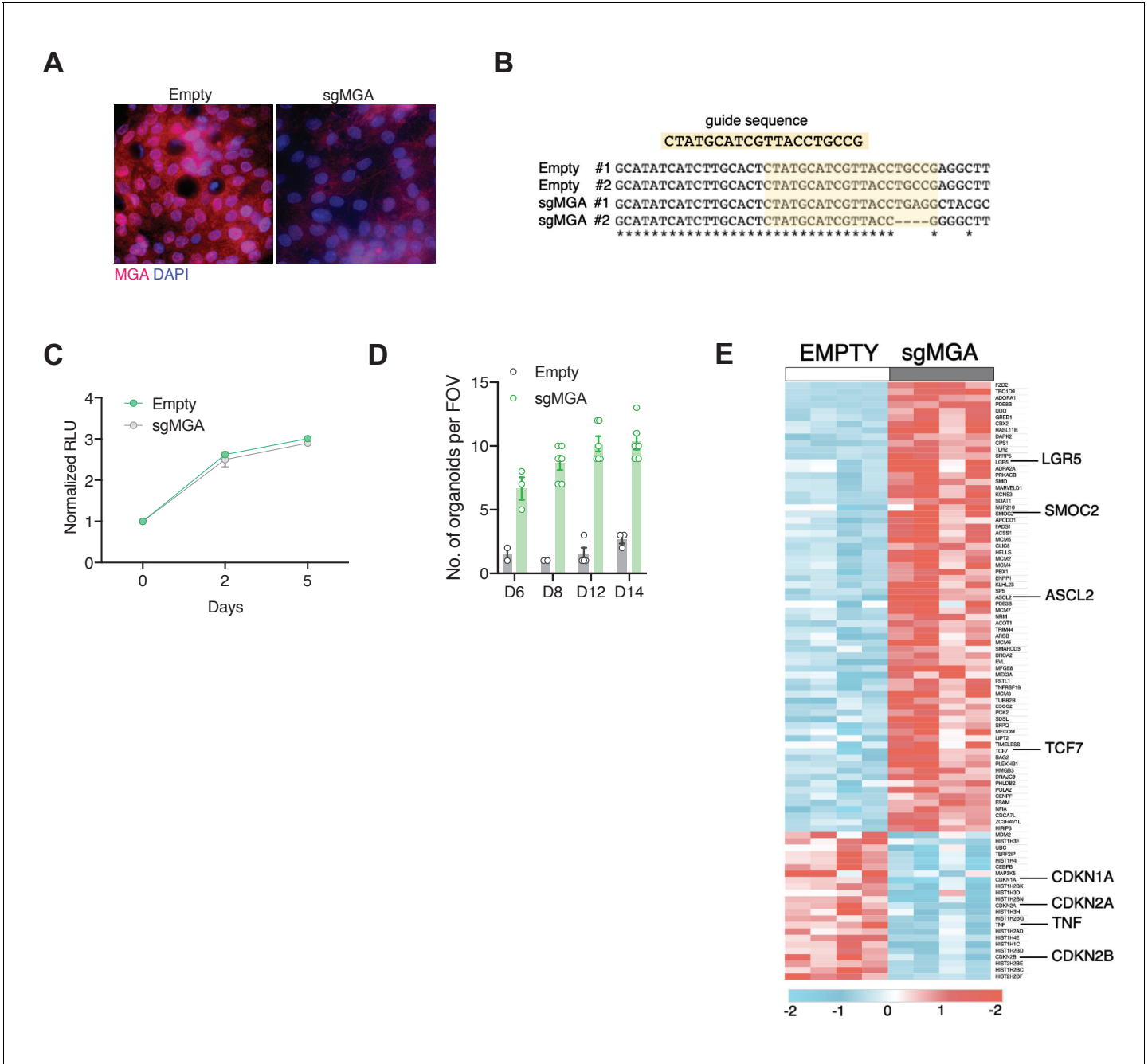


Figure 8—figure supplement 1. MGA has tumor suppressive functions in colon cancer. (A) Immunofluorescent staining for MGA in 2D organoid cultures. (B) Sequencing to show indel formation in clonal sgMGA (#1 and #2) organoids compared to Empty vector transduced controls. (C) Growth of sgMGA and Empty organoids in 2D culture. (D) Timewise comparison of organoid growth of Empty and sgMGA transduced cells after single-cell seeding. (E) Heatmap showing colon cancer stem cell signature genes and senescence associated genes that are differentially expressed between Empty and sgMGA colon organoids (LFC > 1.5, FDR < 0.05).